International Journal of Solids and Structures xxx (2015) xxx–xxx

Contents lists available at ScienceDirect

International Journal of Solids and Structures

journal homepage: www.elsevier.com/locate/ijsolstr

A micromechanical analysis of the fracture properties of saturated porous media

Mingchao Liu, Changqing Chen *

Department of Engineering Mechanics, CNMM & AML, Tsinghua University, Beijing 100084, China

ARTICLE INFO

Article history:
Received 5 August 2014
Received in revised form 3 February 2015
Available online xxxx

Keywords:
Saturated porous medium
Micromechanical model
Stress intensity factor
Fracture toughness

ABSTRACT

A two-dimensional single edge crack problem is employed to investigate the fracture behavior of saturated poroelastic media. The media are mimicked by a micromechanical model consisting of elastic matrix and square arrays of voids with prescribed uniform pore pressure. Finite element method is used to simulate the fracture responses of the model subject to remote stress and pore pressure loading. The stress extrapolation method is extended for the porous media to calculate the nominal stress intensity factor (SIF) from the crack tip stress field. By adopting the tensile strength criterion and assuming either brittle or ductile failure of the constituent solid skeleton of the porous media, lower and upper bounds of the fracture toughness are obtained. Theoretical expressions for the stress intensity factor and the toughness are derived, agreeing well with numerical results. The effects of the arrangement of pores and the non-uniform pore pressure on the cracking of porous media are discussed and are found to only have moderate effects on the obtained results.

© 2015 Elsevier Ltd. All rights reserved.

1. Introduction

Porous media, such as wood, bone, sedimentary rock, and hydrogel, are widely available in nature and modern industry. Their microstructures usually contain both a solid skeleton and a moving pore fluid (either gas or liquid). A strong coupling may exist between the fluid flow and the elastic deformation of the solid skeleton (Biot, 1941; Rice and Cleary, 1976; Detournay and Cheng, 1993; Coussy, 2011). Under external loadings, the fracture of porous media is typically multiphysics coupled (Rice and Simons, 1976; Rudnicki, 2001; Exadaktylos, 2012). Furthermore, the microstructures, such as pores and micro cracks, have been found to have great effects on the mechanical behavior of porous media, especially the fracture behavior (Shafiro and Kachanov, 1997; Cramer and Sevostianov, 2009; Ponson, 2009; Nara et al., 2011, 2014; Ryvkin and Aboudi, 2011; Tokiwa et al., 2013; Tsusaka and Tokiwa, 2013; Zybell et al., 2014). A mutual understanding of the fracture behavior of porous media is of fundamental importance in fulfilling their applications and has received an increasing interest in recent years (Kovalyshen, 2010).

A number of theories have been developed for the elastic and non-elastic deformation of porous media (e.g., Biot, 1941; Rajagopal, 1995; Carmeliet et al., 2013). Among them, the theory of poroelasticity developed by Biot (1941) is well recognized in studying the elastic deformation of porous media. In its classical form, the theory is based on the principle of effective stress and the Darcy's law. The interaction between the pore fluid and solid skeleton is described through the pore pressure. Based on Biot's theory, Rice and Cleary (1976) reformulated the linear constitutive equations by using the more familiar constants (e.g. Poisson's ratio and Bulk modulus). Solutions of several typical poroelasticity problems were also obtained.

With the development of the poroelasticity, numerous studies indicate that the linear quasi-static poroelastic model be useful in a great variety of fields, such as materials engineering, geomechanics and biomechanics (Detournay and Cheng, 1993; Wang, 2000; Hong et al., 2008; Vermorel and Pijaudier-Cabot, 2014). For these fields, fracture problems are common and important, such as hydraulic fracture, bone fracture etc. Accordingly, initiation and extension of cracks in porous media is an area of both practical and theoretical interest (Kovalyshen, 2010; Barani and Khoei, 2014). For porous media, not only the external loadings but also the fluid pressure within pores promotes initial propagation of cracks. The flow of the pore fluid will be affected by the deformation of the solid skeleton. Meanwhile, the material properties of the solid can be changed with the diffusion of the fluid into the solid skeleton (Nara et al., 2012; Duda and Renner, 2013).

Based on the poroelasticity established by Biot (1941), Rice and his coworkers (Rice and Cleary, 1976; Rice and Simons, 1976)

* Corresponding author. Tel./fax: +86 10 62783488.
E-mail address: chencq@tsinghua.edu.cn (C. Chen).

http://dx.doi.org/10.1016/j.ijsolstr.2015.02.031
0020-7683/© 2015 Elsevier Ltd. All rights reserved.

Please cite this article in press as: Liu, M., Chen, C. A micromechanical analysis of the fracture properties of saturated porous media. Int. J. Solids Struct. (2015), http://dx.doi.org/10.1016/j.ijsolstr.2015.02.031

investigated the fracture behavior of a quasi-static semi-infinite shear crack in saturated porous media. Various boundary conditions of the pore pressure on the crack faces were considered and analytical solutions were obtained. Atkinson and Craster (1991) and Craster and Atkinson (1992) employed the integral transformation method to investigate the Mode I and II cracks embedded in poroelastic media. The crack tip pore pressure and stress fields were analytically obtained for both permeable and impermeable crack face boundary conditions. The effects of boundary conditions upon the stress intensity factor (SIF) and energy release rate were also quantified. Radi et al. (2002) considered the steady state crack growth in elastic–plastic porous media. In addition, studies of the thermally activated fracture in porous media were reported by Guarino and Ciliberto (2011).

As a typical example of poroelastic fracture, the problem of a stationary hydraulic fracture in a poroelastic medium is important in the unconventional oil and gas industry (Kovalyshen, 2010; Shojaei et al., 2014). A self-similar analytical plane strain solution for a hydraulic fracture propagating in a poroelastic media was obtained by Lenoach (1995). Adachi and Detournay (2008) presented an analysis of a hydraulic fracture embedded in permeable rock and obtained a multi-scale asymptotic solution of the crack-tip fields. A review of contributions in this area can be found in Huang et al. (2012).

The fracture behavior of porous media are complicated. In general, theoretical solutions are only available for limited boundary value problems. Consequently, numerical simulation methods, such as the finite element method (FEM) was employed to deal with more general poroelastic problems (Lewis and Schrefler, 1998; Ferronato et al., 2010). FEM has been successfully applied in the solution of problems in poroelasticity, especially in poroelastic fracture analysis (Adachi et al., 2007; Selvadurai and Mahyari, 1998; Shao et al., 2014). Selvadurai and Mahyari (1998) studied the plane strain steady crack extension in poroelastic media, in which the Galerkin technique was used and the SIF and the pore pressure fields ahead of crack front were successfully predicted. Recently, Shao et al. (2014) proposed an advanced numerical model to investigate the influence of heat transfer and fluid flow on crack propagation in multi-layered porous materials, with the extended Finite Element Method (XFEM).

In addition to theoretical and numerical studies, a number of experimental studies were conducted to improve our understanding on the fracture properties of porous media. For instance, Nara and his co-workers (2011, 2012, 2013, and 2014) reported experimental investigations on the influence of environmental factors (e.g., relative humidity, temperature, and electrolyte concentration) on the fracture behavior of rock, showing that crack growth in rock is greatly affected by the environmental factors. In addition, Huang et al. (2014) presented an experimental study for crack propagation in claystones to provide useful information for numerical simulation.

In the aforementioned studies, porous media are mostly treated as continuous media, with the influences of the microstructure ignored. In fact, the microstructure around the crack tip may have significant effects on the fracture properties (Shafiro and Kachanov, 1997; Cramer and Sevostianov, 2009; Ryvkin and Aboudi, 2011; Zybell et al., 2014). For example, Bazant (1984) discovered that the crack tip of concrete and rock was blunted by the existing of micro cracks (or pores). Similar effects were found in ductile metal because of the plastic zone. Smith (2005) showed that the role of pore located in the crack tip couldn't be ignored, regardless of how small it was. It's the so-called keyhole problem. Further study indicated that, when the pores exist at the crack tip, there exists competition between at least two mechanisms of a nominal toughness enhancement due to the crack blunting by the presence of pores and the weakening effect caused by the increasing volume fraction of pores (Leguillon and Piat, 2008). Although most of the aforementioned studies are on traditional continuous solids, their conclusions are believed to have implications on porous media. In saturated porous media, the microstructures, especially those located at the crack tip, can affect the fracture toughness and crack propagation of the porous media significantly. Therefore, it is desirable to quantify the fracture behavior of porous media, such as the influence of the microstructure and the coupling of fluid and solid on the fracture characteristics.

In this paper, a two dimensional micromechanical model is presented, which is capable of describing the influence of the microstructure of the solid skeleton, and the coupling of the fluid flow and the deformation of the solid skeleton. In this model, the interaction between fluid and solid is described by the pore pressure p, and the influence of the diffusion of fluid into solid skeleton is ignored. Based on the theory of linear fracture mechanics, theoretical expressions of the fracture parameters (e.g., SIF and fracture toughness) of porous media are obtained. In addition, the parameters are calculated numerically using FEM. The accuracy of the assumptions adopted in this model is discussed by varying the arrangement of the pores and the distribution of pore pressure. Finally, a few conclusions are drawn.

2. Micromechanical model

To investigate the fracture characteristics of saturated porous media, a two dimensional plane strain edge crack problem is considered, as shown in Fig. 1, where the porous medium is mimicked by periodically distributed pores embedded in an elastically brittle solid. A rectangular coordinate system oxy centered at the crack tip is defined and the geometrical parameters are also shown in Fig. 1, with a being the crack length, w and b being the specimen width and height, respectively, d being the pore diameter, and l being the lattice constant. Accordingly, the porosity is given by

$$\varphi = \pi d^2/4l^2 \tag{1}$$

It is noted that the pores in most porous media may have varying shapes and sizes and can be randomly distributed, giving rise to macroscopically isotropic behavior. For simplicity, the following assumptions are adopted in the model:

(i) The pores are circular and of the same size and are arranged in square arrays.
(ii) The saturated fluid in all pores is modeled by a prescribed constant pressure p. The effect of deformation upon p is neglected.
(iii) The crack is straight and passes through the centers of pores.

In addition to the square arrays of pores in Assumption (i), the effects of a different distribution of triangular arrays of pores upon the fracture behavior will be discussed later. Moreover, the pore pressure p in a porous medium is generally coupled with deformation. Assumption (ii) implies that only unidirectional coupling is considered here (i.e., p affects deformation, but not vice versa). As to Assumption (iii), it can be justified as follows. Note that the cross section between two pore centers is weakest. It can therefore be expected that crack advances along the weakest section. In addition to a remote uniaxial uniform loading σ_∞, the crack faces are also subject to pressure p.

3. Theoretical analysis

3.1. Stress intensity factor

According to linear elastic fracture mechanics (LEFM), the SIF in mode I of a homogenous elastic counterpart of Fig. 1 is given by

Please cite this article in press as: Liu, M., Chen, C. A micromechanical analysis of the fracture properties of saturated porous media. Int. J. Solids Struct. (2015), http://dx.doi.org/10.1016/j.ijsolstr.2015.02.031

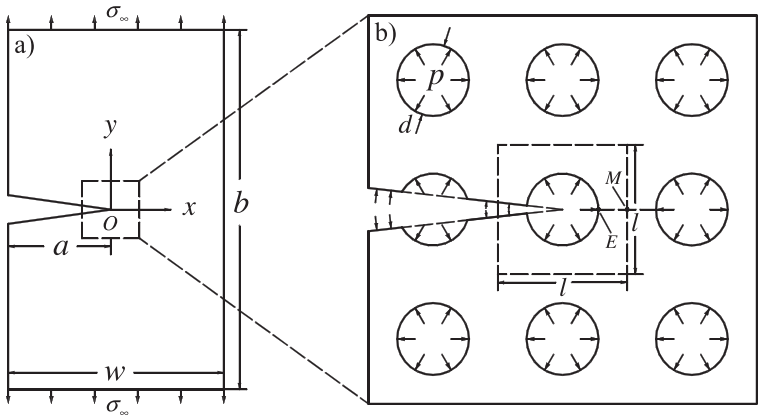

Fig. 1. Schematic of an edge crack in a porous medium with the square arrays of pores: (a) Macroscopic specimen with remote stress σ_∞; (b) Illustration of the square arrays of pores with uniform pressure p imposed upon the pores and crack faces. A unit cell with a single pore of diameter d and lattice constant l is also shown.

$$K_{\mathrm{I}} = \lim_{r\to 0}\sqrt{2\pi r}\sigma_{yy} \quad (r>0,\ \theta=0) \tag{2}$$

where $\sigma_{yy}(r>0,\ \theta=0)$ is the y-direction normal stress along the crack propagation direction. For an elastic edge crack problem subject to remote stress σ_∞, K_{I} has the form of

$$K_{\mathrm{I}} = \sigma_\infty\sqrt{\pi a}\cdot f(\eta), \quad \eta = a/w \tag{3}$$

where $f(\eta)$ is the geometry factor given by (Tada et al., 2000)

$$f(\eta) = 1.12 - 0.23\eta + 10.56\eta^2 - 21.74\eta^3 + 30.42\eta^4 \tag{4}$$

For the single edge crack problem of the homogenized linear elastic porous medium given in Fig. 1, the macroscopic crack tip fields are much more complicated than those of linear elastic solids. However, it has been shown by Atkinson and Craster (1991), Loret and Radi (2001) and Hui et al. (2013), among others that the same singularity of $-1/2$ exists for porous media. Because the problem in Fig. 1 is linear, the effects of remote stress σ_∞ and pore pressure p on SIF can be superimposed. Analogous to elastic solids, the macroscopic crack tip stresses $\langle\sigma_{ij}\rangle$ for a porous medium in Mode I can be related to a nominal stress intensity factor $\langle K_{\mathrm{I}}\rangle$ by

$$\langle\sigma_{ij}\rangle = \frac{\langle K_{\mathrm{I}}\rangle}{\sqrt{2\pi r}}\cdot\Sigma_{ij}(\theta), \quad i,j=x,y \tag{5}$$

where $\Sigma_{ij}(\theta)$ is the angular functions the same as those for elastic solids. Extending the LEFM theory to porous media by superimposing the effects, $\langle K_{\mathrm{I}}\rangle$ can be assumed to be

$$\langle K_{\mathrm{I}}\rangle = \{\sigma_\infty\cdot f_\sigma(\eta,\varphi) + p\cdot f_p(\eta,\varphi)\}\cdot\sqrt{\pi a}. \tag{6}$$

with $f_\sigma(\eta,\varphi)$ and $f_p(\eta,\varphi)$ being functions to be determined. First, consider only the remote stress loading. For a homogenized elastic porous medium with $p=0$, its macroscopic Young's modulus $\langle E\rangle$ and Poisson's ratio $\langle\nu\rangle$ vary with the porosity φ. Note that the planar K_{I} in Eq. (2) for isotropic elastic solids is independent of the elastic constants (i.e., Young's modulus E and Poisson's ratio ν). Therefore, the nominal stress intensity factor $\langle K_{\mathrm{I}}\rangle$ for homogenized isotropic elastic porous media should also be independent of $\langle E\rangle$ and $\langle\nu\rangle$ and thus has no dependence upon the porosity φ. Otherwise, a porosity dependent $\langle K_{\mathrm{I}}\rangle$ indicates that it is a function of $\langle E\rangle$ and $\langle\nu\rangle$. That is

$$f_\sigma(\eta,\varphi) = f_\sigma(\eta). \tag{7}$$

Moreover, the geometry factor $f_\sigma(\eta)$ for homogenized elastic porous media should be the same as that of elastic solids $f(\eta)$, that is

$$f_\sigma(\eta) = f(\eta). \tag{8}$$

In the case of pressure loading only, contribution from the pore pressure field near the crack face instead of the overall pore pressure dominates $\langle K_{\mathrm{I}}\rangle$ (the dominance will be verified by FEM in the following section). Following the same argument applied to $f_\sigma(\eta,\varphi)$ due to the remote stress loading, the independence of $\langle K_{\mathrm{I}}\rangle$ upon porosity means that $f_p(\eta,\varphi)$ for the pore pressure be also independent of porosity, giving $f_p(\eta,\varphi) = f_p(\eta)$. Note that, both f_σ and f_p in Eq. (6) are the geometrical factors in SIF. For conventional elastic solids, the geometrical factors associated with remote stressing and crack face pressure loading are the same. One can thus expect that f_σ and f_p for the homogenized porous media are close to each other, if not identical. Based upon above argument, $f_p(\eta,\varphi)$ can be approximated by

$$f_p(\eta,\varphi) = f_p(\eta) = f(\eta). \tag{9}$$

Therefore, $\langle K_{\mathrm{I}}\rangle$ can be re-expressed as

$$\langle K_{\mathrm{I}}\rangle = (\sigma_\infty + p)\sqrt{\pi a}\cdot f(\eta). \tag{10}$$

It should be noted that, although the porosity φ has no effect upon the nominal SIF $\langle K_{\mathrm{I}}\rangle$, it does have significant effect upon the local stress σ^l_{ij} in the solid skeleton. In fact, as shown by Smith (2005), the size and distribution of pores close to the crack tip affect the fracture behavior greatly. Such a phenomenon is also referred to as key-hole problem (Leguillon and Piat, 2008). In general, the local stress in the solid skeleton dictates the cracking of porous media and is important in evaluating the toughness of porous media. As a first order approximation, the crack tip local stress σ^l_{ij} is assumed to be defined by a local stress intensity factor K^l_{I} as

$$\sigma^l_{ij} = \frac{K^l_{\mathrm{I}}}{\sqrt{2\pi r}}\cdot\Sigma^l_{ij}(\theta), \quad i,j=x,y \tag{11}$$

where superscript "l" refers to local quantities, $\Sigma^l_{ij}(\theta)$ are angular functions with $\Sigma^l_{yy}(0)=1$, and K^l_{I} is assumed to related to $\langle K_{\mathrm{I}}\rangle$ by

$$K^l_{\mathrm{I}} = \langle K_{\mathrm{I}}\rangle\cdot g(\varphi). \tag{12}$$

Here, the porosity factor $g(\varphi)$ represents the effect of porosity upon the local stress fields. For the square arrays of uniform circular pores given in Fig. 1, $g(\varphi)$ can be estimated as follows.

Within each unit cell ahead of the crack tip, equilibrium in the y direction indicates that the equivalent macroscopic stress $\langle\sigma_{yy}\rangle$

Please cite this article in press as: Liu, M., Chen, C. A micromechanical analysis of the fracture properties of saturated porous media. Int. J. Solids Struct. (2015), http://dx.doi.org/10.1016/j.ijsolstr.2015.02.031

along the crack line $y = 0$ is related to the local stress σ^l_{yy} in the solid skeleton by

$$\int_U \langle\sigma_{yy}\rangle(x, y = 0)\mathrm{d}x = \int_S \sigma^l_{yy}(x, y = 0)\mathrm{d}x. \tag{13}$$

where the integral paths S and U refer to the cross section of the solid skeleton and the entire unit cell, respectively. According to the Intermediate Value Theorem (IVT), Eq. (13) can be expressed further on unit cell level as

$$\langle\bar{\sigma}_{yy}\rangle \cdot l = \bar{\sigma}^l_{yy} \cdot (l - d) \tag{14}$$

where $\langle\bar{\sigma}_{yy}\rangle$ and $\bar{\sigma}^l_{yy}$ are the corresponding average values of $\langle\sigma_{yy}\rangle$ and σ^l_{yy} along $y = 0$ with the unit cell.

Note that $\langle\bar{\sigma}_{yy}\rangle$ and $\bar{\sigma}^l_{yy}$ comply with Eqs. (5) and (11). One can get the following relation between $\langle K_\mathrm{I}\rangle$ and K^l_I from Eqs. (5), (11) and (14) as

$$\langle K_\mathrm{I}\rangle = K^l_\mathrm{I} \cdot \frac{l - d}{l}. \tag{15}$$

Combining Eqs. (1), (12) and (15), the porosity factor for the square arrays of voids can be estimated to be

$$g(\varphi) = 1/(1 - 2\sqrt{\varphi/\pi}). \tag{16}$$

Consequently, the equivalent local stress (i.e., Eq. (11)) in the solid skeleton and along the crack line is given by

$$\sigma^l_{yy} = \frac{\langle K_\mathrm{I}\rangle}{\sqrt{2\pi r}} \cdot g(\varphi) \tag{17}$$

3.2. Fracture toughness

In general, the fracture behavior of porous media is controlled by the properties of the constituent solid. Here, it is assumed that crack growth is by means of breaking of the elastic solid skeleton, for which two failure modes (i.e., brittle and ductile failure) are considered. For brittle failure, as a rule of thumb, it is assumed that crack starts to advance when the maximum stress (normally, the stress σ^{lE}_{yy} at the edge point E of the cross section, as labeled in Fig. 1) reaches its failure strength σ_{fs}. On the other hand, ductile failure is deemed to occur when the porous medium fails via the average stress of the cross section ahead the crack tip (approximated by the stress at the middle point M, i.e., σ^{lM}_{yy}) reaching the failure strength σ_{fs}.

To evaluate the local stress σ^{lE}_{yy} as shown in Fig. 1, two effects must be taken into account: First, the local stress field solely due to the crack; Second, the stress concentration effect due to the lead pore. Consequently, σ^{lE}_{yy} can be expressed as

$$\sigma^{lE}_{yy} = \left(\frac{\langle K_\mathrm{I}\rangle}{\sqrt{2\pi r}} \cdot S_t\right)\Big|_{r=d/2} = \frac{\langle K_\mathrm{I}\rangle}{\sqrt{\pi d}} \cdot S_t. \tag{18}$$

where S_t is the stress concentration factor of a circular hole in a plate of finite width. It is noted that the pores are distributed evenly ahead the crack. From a unit cell point of view, each pore can be viewed as a pore of diameter d embedded in a finite plate of width l (see Fig. 1). Accordingly, S_t can be approximated as (Heywood, 1952)

$$S_t = 2\left(1 - \frac{d}{l}\right)^{-1} + \left(1 - \frac{d}{l}\right)^2 \tag{19}$$

which increases from 3 monotonically with d/l increasing.

When the local stress σ^{lE}_{yy} reaches its failure stress σ_{fs}, the corresponding toughness of brittle failure is given by substituting Eq. (19) into (18) as

$$\langle K^B_\mathrm{IC}\rangle = \sigma_{fs}\sqrt{\pi l} \cdot \sqrt{\frac{d}{l}} \cdot \frac{1}{S_t} \tag{20}$$

where superscript "B" denotes brittle failure. It is noted that the second and third parts of the right hand side of Eq. (20) represent the two mechanisms of blunting and stress concentration effects, respectively. When the blunting effect prevails, the toughness associated with the brittle failure increases with porosity. However, the toughness is expected to decreases with porosity when the latter effect dominates. Therefore, the competition of the two mechanisms indicates the existence of a peak toughness with varying porosity

For the ductile failure mode, the stress at the middle point M cannot be obtained by simply extending Eq. (18) to $r = l/2$. In fact, we have shown in Section 3.1 that the equivalent local stress at the middle point M in the solid skeleton complies with Eq. (17), i.e.,

$$\sigma^{lM}_{yy} = \left(\frac{\langle K_\mathrm{I}\rangle}{\sqrt{2\pi r}} \cdot g(\varphi)\right)\Big|_{r=l/2} = \frac{\langle K_\mathrm{I}\rangle}{\sqrt{\pi l}} \cdot g(\varphi) \tag{21}$$

With the local stress σ^{lM}_{yy} equal to the failure stress σ_{fs}, the toughness of the porous media in ductile failure can be derived as

$$\left\langle K^D_\mathrm{IC}\right\rangle = \sigma_{fs} \cdot \sqrt{\pi l} \cdot (1 - 2\sqrt{\varphi/\pi}) \tag{22}$$

where superscript "D" denotes ductile failure. Eq. (22) is derived from the specific case of square arrays of circular pores shown in Fig. 1. Using a hexagonal honeycomb model, Gibson and Ashby (1999) obtained the in-plane fracture toughness as

$$\left\langle K^G_\mathrm{IC}\right\rangle = C_1 \cdot \sigma_{fs}\sqrt{\pi l} \cdot (1 - \varphi)^2 \tag{23}$$

It can be seen that the fracture toughness K_{Ic} is related to the yield strength of the solid skeleton σ_{fs}, the unit cell size of microstructure l, and the porosity φ.

4. Finite element simulations

In order to verify the theoretical analyses given in Section 3, the microscopic crack tip fields are also obtained numerically with the commercially available finite element software package ANSYS. The solid skeleton of the model is meshed with 8-node biquadratic plane strain elements (i.e., Solid Quad 8Node 82 element in ANASYS). Due to symmetry, only half of the model ($y > 0$) in Fig. 1(a) is meshed and symmetrical boundary conditions are enforced along ($y = 0$ and $x > 0$). The constituting solid skeleton is assumed to be linear elastic with Young's modulus $E = 70$ GPa and Poisson ratio $v = 0.3$.

It should be pointed out that the model in Fig. 1 is employed to mimic a homogenous porous medium with a crack by using FEM. In theory, the number of pores in each dimension should be big enough to eliminate any size effect. Nevertheless, increasing the number of pores in the model means increased number of degrees of freedom and computational cost. Therefore, a trade-off between the pore number and numerical efficiency must be sought. Numerical experiment shows that a model with the number of unit cells of 30×30 is sufficient to show the homogenized responses of porous media. Therefore, all finite element models in this study have 30×30 pores. Moreover, mesh sensitivity study has been conducted to ensure the numerical convergence of the models. Graded meshes are employed for the crack tip region. The total degrees of freedom of a typical mesh is about 200,000.

4.1. The stress extrapolation method for determining SIF

Once the microscopic crack tip fields (i.e., stress and displacement) are obtained, the macroscopic fracture characteristics (e.g.,

Please cite this article in press as: Liu, M., Chen, C. A micromechanical analysis of the fracture properties of saturated porous media. Int. J. Solids Struct. (2015), http://dx.doi.org/10.1016/j.ijsolstr.2015.02.031

SIF and fracture toughness) can be derived. As shown by Atkinson and Craster (1991), Loret and Radi (2001) and Hui et al. (2013), the crack tip stress fields of porous media show the same singularity as those of linear elastic solids. The stress extrapolation method to obtain SIF of conventional solids (Kim and Eberhardt, 1997) is adapted here for porous media.

Considering the localized feature of the singularity and the Williams series for LEFM (Anderson, 2005), an apparent stress intensity factor $\tilde{K}_I$ for the crack problem subject to remote stress in Fig. 1 is defined in order to extrapolate K_I at $r = 0$

$$\sigma_{yy} \cdot \sqrt{2\pi r}\Big|_{\theta=0} \triangleq \tilde{K}_I = K_I + \sigma_\infty \cdot (c_1 r^{1/2} + c_2 r). \tag{24}$$

where c_1 and c_2 are constants to be determined and higher order terms are ignored. In the original method of Kim and Eberhardt (1997), only a constant term and a linear term in r are included (i.e., $c_1 = 0$ in Eq. (24) is assumed). However, it is found in this study that, although the additional nonlinear term $r^{1/2}$ has only minor effect for continuum solids, it is vital to ensure the repeatability of the stress extrapolation method for porous media.

Fig. 2(a) shows the calculated local stress σ^l_{yy} along the crack line for the model in Fig. 1 with σ_∞ and $p = 0$ (denoted by lines). The porosity is about 19.6%. It is clear that, owing to the existence of the pores, the stress does not vary continuously across pores. In general, the stress decreases from the left end of each cross section between two adjacent pores and reach its minimum at a point close to the middle point. Also shown in Fig. 2(a) is the stress averaged over each cross section, represented by solid symbols at the middle points of the cross sections. The calculated average local stresses over the cross sections in Fig. 2(a) are re-plotted in Fig. 2(b) in terms of the apparent stress intensity factor $\tilde{K}_I$ versus r/l. Curve fitting the results in Fig. 2(b) with Eq. (24) and extrapolating to $r/l = 0$ give the remote stress induced local stress intensity factor K^l_I, as discussed in Section 3.1.

When only pore pressure p is present, the induced stress intensity factor can be obtained in a way analogous to the loading case of remote stressing only, i.e.,

$$\sigma_{yy} \cdot \sqrt{2\pi r}\Big|_{\theta=0} \triangleq \tilde{K}_I = K_I + p \cdot (c_3 r^{1/2} + c_4 r). \tag{25}$$

where c_3 and c_4 are unknown constants. For any combinations of loadings σ_∞ and p, the stress intensity factor can be obtained similarly as the superimposed principle applies for the linear elastic problems considered in this paper. By varying the porosity in the FE model, the dependence of K^l_I on φ (i.e., $g(\varphi)$ in Eq. (12)) can then be obtained numerically.

4.2. Toughness associated with brittle and ductile failure modes

From the numerical results of crack tip stress field, the fracture toughness can also be evaluated. For the brittle failure mode, the corresponding toughness K^B_{IC} is obtained by choosing the loadings so that the maximum local stress σ^{lE}_{yy} is equal to the failure stress σ_{fs} while the toughness K^D_{IC} for the ductile failure mode is derived when the local stress σ^{lM}_{yy} at the cross section middle point reaches σ_{fs}. Mathematically, they can be expressed as

$$K^B_{IC} = \frac{\sigma_{fs}}{\sigma^{lE}_{yy}} \cdot \langle K_I \rangle \tag{26}$$

and

$$K^D_{IC} = \frac{\sigma_{fs}}{\sigma^{lM}_{yy}} \cdot \langle K_I \rangle \tag{27}$$

where $\langle K_I \rangle$ is the nominal stress intensity factor given in Eq. (10).

5. Numerical results

The FE method predicted local SIF K^l_I due to remote stress and pore pressure are shown in Fig. 3 as solid symbols. Also included are the theoretical results given by Eq. (16), represented by line. Note that the results in Fig. 3 are normalized by the nominal SIF $\langle K_I \rangle$, giving the porosity factor $g(\varphi)$ in accordance with Eq. (12). It is seen from Fig. 3 that the porosity factor $g_\sigma(\varphi)$ due to remote stress is slight higher than $g_p(\varphi)$ associated with only pore pressure. Note from Fig. 1 that there exists a crack tip hole in the model which slightly reduces the crack tip singularity. The reduction is in fact more pronounced for pore pressure loading than remote stress loading, giving rise to a slightly higher $g_\sigma(\varphi)$ than $g_p(\varphi)$. Nevertheless, both agree with each other very closely and can be approximated by a single function (i.e., the theoretical expression (16)). Moreover, Fig. 3 shows that the porosity factor increases with increasing porosity, which means the local SIF of porous media becomes larger as the porosity increases. Furthermore, the porosity factor reduces to 1 when the porosity is equal to zero, indicating the porous model reduces to continuum media without pores.

The FE predicted porosity dependent fracture toughness of the porous medium is shown in Fig. 4 as up and down triangles for the brittle and ductile failure modes, respectively. The corresponding theoretical predictions given by Eqs. (20) and (22) are included as dotted and dot-dash lines for the purpose of comparison. The Huang-Gibson results in Fig. 4 is for regular hexagonal honeycombs

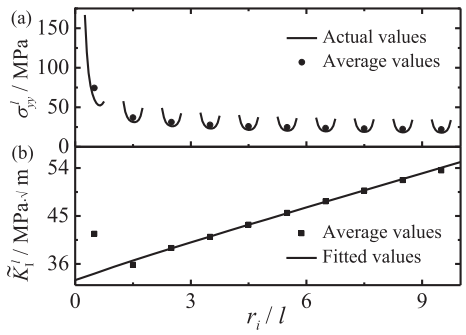

Fig. 2. Illustration of using the stress extrapolation method to determine the stress intensity factor. (a) FE calculated local stress and its corresponding cross section average values along the crack line; (b) Curve fitting the apparent stress intensity factor with Eq. (24). The results are shown for a model with cell numbers of 30 × 30, crack length a/l = 4.5, porosity φ = 19.6%, and loading σ_∞ = 10 MPa and p = 0.

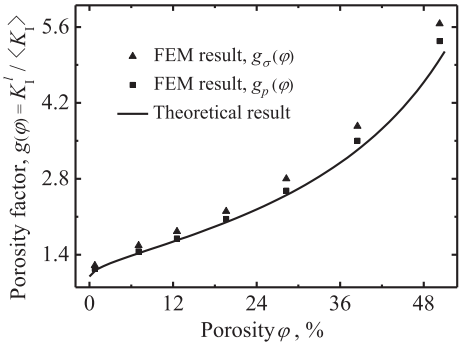

Fig. 3. Comparison of FE and theoretical predictions of the local SIFs K^l_I due to the remote stress and pore pressure. Here, normalized values are presented for a model with cell numbers of 30 × 30, and the loading are σ_∞ = 10 MPa and p = 10 MPa, respectively.

Please cite this article in press as: Liu, M., Chen, C. A micromechanical analysis of the fracture properties of saturated porous media. Int. J. Solids Struct. (2015), http://dx.doi.org/10.1016/j.ijsolstr.2015.02.031

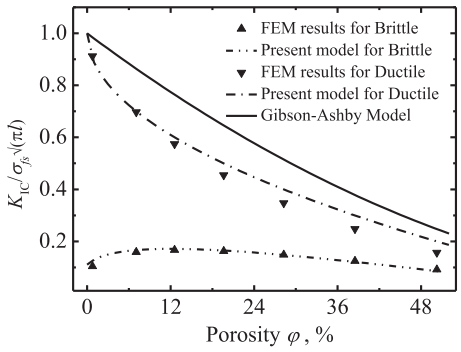

Fig. 4. Predicted fracture toughness of the porous media as a function of porosity. The FE and theoretical results of brittle and ductile failure modes are both included. The hexagonal honeycomb model (Gibson and Ashby, 1999) is also contained for comparison. Cell numbers of the FE model is 30 × 30, and loading is σ_∞ = 10 MPa and p = 0.

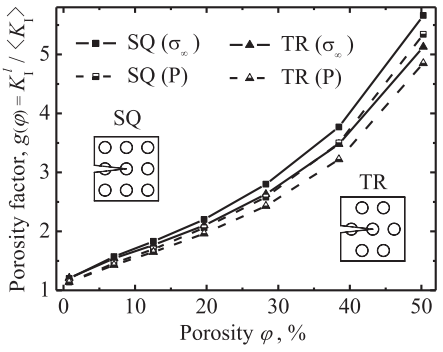

Fig. 5. Effects of square (SQ) and triangle (TR) arrangements of pores upon local stress intensity factors for both remote stress and pressure loading. The normalized SIFs are presented for a model with cell numbers of 30 × 30, loading σ_∞ = 10 MPa and p = 10 MPa.

and serves as reference only. Overall, excellent agreement between the FE and theoretical predictions of the fracture toughness is achieved for both failure modes. For the brittle failure mode, the FE results indeed show that the toughness first increases and then decreases with increasing porosity, due to the two competition mechanisms of crack tip blunting and stress concentration effects predicted by Eq. (20) for the existence of pores. A similar feature has been reported by Ryvkin and Aboudi (2011) for a double periodic voided media. For the ductile failure mode, the FE and theoretical predictions show that the corresponding toughness decreases with porosity. In fact, the solid skeletons of real porous media may not fail by ideal brittle or ductile. In such cases, their toughness are expected to lie in the region between the brittle and ductile failure modes in Fig. 4. With the established SIF and fracture toughness, the following fracture criterion of porous media can be established as

$$\langle K_I \rangle \geqslant K_{Ic}. \tag{28}$$

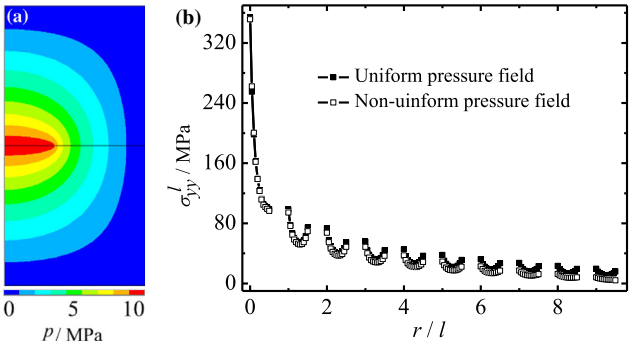

Fig. 6. The cracked plane of a porous medium: (a) Calculated pressure profile of non-uniform distribution with boundary condition of prescribed pressure of 10 MPa on the crack face, impermeable condition on left boundary, and zero pressure for other boundaries; (b) Calculated crack tip stress distribution of the cracked plane with the calculated pressure field. The results are shown for a model with crack length a/l = 10.5 and porosity φ = 19.6%.

6. Discussions

6.1. Effects of different arrangements of pores

Generally, pores are randomly distributed in most natural and manmade porous media. To simplify the analysis, square (SQ) arranged pores are assumed in previous sections. Here, we discuss the effects of a different arrangement of pores, i.e., triangle (TR) arrangement. The FE calculated SIFs corresponding to remote stress and pore pressure loadings are given in Fig. 5 for various porosities, shown again as the normalized SIF (i.e., porosity factor $g(\varphi)$). One can see that the porosity factor is only moderately sensitive to the arrangement of pores.

6.2. Non-uniform pressure field

In the model given in Fig. 1, uniform pore pressure is adopted. In porous media, the pore pressure for the crack problem is, in general, position dependent (Exadaktylos, 2012). For a simplified unidirectional coupling model neglecting the effect of deformation upon fluid flow, the pressure field can then be approximated by solving the equation $\nabla^2 p = 0$. Now, re-consider the crack problem shown in Fig. 1, with the continuum modeled by the simplified poroelasticity in conjunction with prescribed pressure of 10 MPa on the crack face, impermeable condition on left boundary, and zero pressure for other boundaries. The numerically calculated pore pressure is shown in Fig. 6(a). One can see that the pore pressure in the cracked poroelastic solid is *not* uniform. Subsequently, the assumed uniform pore pressure in Section 4 is replaced by the calculated non-uniform pore pressure. The purpose is to gauge the effect of uniform pore pressure assumption on the obtained crack tip characteristics.

For the single edge crack problem with $a/w = 0.35$, porosity of 19.6%, and the uniform pore pressure p = 10 MPa replaced by the pore pressure field shown in Fig. 6(b), the calculated local stress σ_{yy}^I along the crack is included in Fig. 6(b) as dotted lines. One can see that the calculated stress using the much simpler uniform pore pressure (see the solid line in Fig. 6(b)) assumption only differs slightly from that with more realistic non-uniform pore pressure, indicating that the contribution from the pore pressure field near the crack face indeed dominates the crack tip behavior – stress intensity factor. This dominance confirms the argument suggested in Section 3.1.

7. Concluding Remarks

The fracture behavior of saturated porous media is investigated by a two dimensional voided micromechanical crack model theoretically and numerically. The interaction between solid skeleton and fluid insides pores are modeled by the assumed uniform constant pore pressure. The stress extrapolation method is adapted to calculate the SIF from the FE simulated local stress field. Theoretical expression of the SIF is obtained and is found to be able to reduce to the degenerated continuous media.

Please cite this article in press as: Liu, M., Chen, C. A micromechanical analysis of the fracture properties of saturated porous media. Int. J. Solids Struct. (2015), http://dx.doi.org/10.1016/j.ijsolstr.2015.02.031

As to the facture toughness, brittle and ductile failures of the elastic solid skeleton constituting the porous media are identified and the corresponding theoretical expressions are proposed. In the case of ductile failure mode, the toughness is found to decrease monotonically with increasing porosity. For the brittle failure mode, however, the toughness first increases and then decreases with porosity increasing, due to the two competition mechanisms of crack tip blunting and stress concentration effects in the presence of pores. The latter indicates that a proper value of porosity can in fact enhance the fracture toughness of porous media. For real porous media, in which the failure mode is between ideal ductile and brittle, their toughness are expected to lie in the region between the lower and upper bound corresponding to brittle and ductile failure modes respectively. Good agreement between the theoretical predictions and numerical results on the SIF and toughness are observed.

To assess the reliability of the obtained results using the simplified assumptions of square arrays of voids and uniform pore pressure, the influence of different arrangements of pores and pressure distributions is discussed. It is found that the SIF only has a moderate sensitivity to the pore arrangement and the crack tip stress field is dictated by the pore pressure field near the crack face. Therefore, any non-uniform pore pressure outside the leading pores is not expected to have a significant effect on the fracture behavior of porous media.

Acknowledgements

The authors are grateful for the financial support of this work by the National Natural Science Foundation of China (No. 11472149), the National Basic Research Program of China (No. 2011CB610305), and the Tsinghua University Initiative Scientific Research Program (No. 2014z22074).

References

Adachi, J.I., Detournay, E., 2008. Plane strain propagation of a hydraulic fracture in a permeable rock. Eng. Fract. Mech. 75, 4666–4694.
Adachi, J., Siebrits, E., Peirce, A., Desroches, J., 2007. Computer simulation of hydraulic fractures. Int. J. Rock Mech. Min. Sci. 44, 739–757.
Anderson, T.L., 2005. Fracture Mechanics: Fundamentals and Applications. CRC Press.
Atkinson, C., Craster, R.V., 1991. Plane strain fracture in poroelastic media. Proc. R. Soc. London Ser. A. 434, 605–633.
Barani, O.R., Khoei, A.R., 2014. 3D modeling of cohesive crack growth in partially saturated porous media: a parametric study. Eng. Fract. Mech. 124–125, 272–286.
Bazant, Z.P., 1984. Size effect in blunt fracture: concrete, rock, metal. J. Eng. Mech. 110, 518–535.
Biot, M.A., 1941. General theory of three-dimensional consolidation. J. Appl. Phys. 12, 155–164.
Carmeliet, J., Derome, D., Dressler, M., Guyer, R.A., 2013. Nonlinear poro-elastic model for unsaturated porous solids. J. Appl. Mech. 80, 020909.
Coussy, O., 2011. Mechanics and Physics of Porous Solids. John Wiley & Sons.
Cramer, M., Sevostianov, I., 2009. Effect of pore distribution on elastic stiffness and fracture toughness of porous materials. Int. J. Fract. 160, 189–196.
Craster, R.V., Atkinson, C., 1992. Shear cracks in thermoplastic and poroelastic media. J. Mech. Phys. Solids 40, 887–924.
Detournay, E., Cheng, AH-D., 1993 (Fundamentals of poroelasticity). In: Hudson (Ed.), Comprehensive Rock Engineering. Pergamon Press, Oxford.
Duda, M., Renner, J., 2013. The weakening effect of water on the brittle failure strength of sandstone. Geophys. J. Int. 192, 1091–1108.
Exadaktylos, G., 2012. A study of the transient fluid flow around a semi-infinite crack. Int. J. Solids Struct. 49, 3323–3334.
Ferronato, M., Castelletto, N., Gambolati, G., 2010. A fully coupled 3-D mixed finite element model of Biot consolidation. J. Comput. Phys. 229, 4813–4830.
Gibson, L.J., Ashby, M.F., 1999. Cellular Solids: Structure and Properties. Cambridge University Press.
Guarino, A., Ciliberto, S., 2011. Thermally activated fracture of porous media. Eur. Phys. J. B 83, 215–221.
Heywood, R.B., 1952. Designing by Photoelastacity. Chapman and Hall, London.
Hong, W., Zhao, X., Zhou, J., Suo, Z., 2008. A theory of coupled diffusion and large deformation in polymeric gels. J. Mech. Phys. Solids 56, 1779–1793.
Huang, J., Griffiths, D.V., Wong, S.W., 2012. Initiation pressure, location and orientation of hydraulic fracture. Int. J. Rock Mech. Min. Sci. 49, 59–67.
Huang, Y., Xie, S.Y., Shao, J.F., 2014. An experimental study of crack growth in claystones. Eur. J. Environ. Civ. Eng. 18, 307–319.
Hui, C.Y., Long, R., Ning, J., 2013. Stress relaxation near the tip of a stationary mode I crack in a poroelastic solid. J. Appl. Mech. 80, 021014.
Kim, B.S., Eberhardt, A.W., 1997. First and second order stress extrapolation for mode I and mode II edge cracks. Eng. Fract. Mech. 57, 715–720.
Kovalyshen, Y., 2010. Fluid-driven fracture in poroelastic medium [Ph.D. thesis], University of Minnesota.
Leguillon, D., Piat, R., 2008. Fracture of porous materials–Influence of the pore size. Eng. Fract. Mech. 75, 1840–1853.
Lenoach, B., 1995. The crack tip solution for hydraulic fracturing in a permeable solid. J. Mech. Phys. Solids 43, 1025–1043.
Lewis, R.W., Schrefler, B.A., 1998. The Finite Element Method in the Static and Dynamic Deformation and Consolidation of Porous Media. John Wiley & Sons.
Loret, B., Radi, E., 2001. The effects of inertia on crack growth in poroelastic fluid-saturated media. J. Mech. Phys. Solids 49, 995–1020.
Nara, Y., Morimoto, K., Yoneda, T., Hiroyoshi, N., Kaneko, K., 2011. Effects of humidity and temperature on subcritical crack growth in sandstone. Int. J. Solids Struct. 48, 1130–1140.
Nara, Y., Morimoto, K., Hiroyoshi, N., Yoneda, T., Kaneko, K., Benson, P.M., 2012. Influence of relative humidity on fracture toughness of rock: implications for subcritical crack growth. Int. J. Solids Struct. 49, 2471–2481.
Nara, Y., Nakabayashi, R., Maruyama, M., Hiroyoshi, N., Yoneda, T., Kaneko, K., 2014. Influences of electrolyte concentration on subcritical crack growth in sandstone in water. Eng. Geol. 179, 41–49.
Nara, Y., Yamanaka, H., Oe, Y., Kaneko, K., 2013. Influence of temperature and water on subcritical crack growth parameters and long-term strength for igneous rocks. Geophys. J. Int. 193, 47–60.
Ponson, L., 2009. Depinning transition in the failure of inhomogeneous brittle materials. Phys. Rev. Lett. 103, 055501.
Radi, E., Bigoni, D., Loret, B., 2002. Steady crack growth in elastic–plastic fluid-saturated porous media. Int. J. Plast. 18, 345–358.
Rajagopal, K.R., 1995. Mechanics of Mixtures. World scientific, Singapore.
Rice, J.R., Cleary, M.P., 1976. Some basic stress diffusion solutions for fluid – saturated elastic porous media with compressible constituents. Rev. Geophy. 14, 227–241.
Rice, J.R., Simons, D.A., 1976. The stabilization of spreading shear faults by coupled deformation-diffusion effects in fluid-infiltrated porous materials. J. Geophy. Res. 81, 5322–5334.
Rudnicki, J.W., 2001. Coupled deformation-diffusion effects in the mechanics of faulting and failure of geomaterials. Appl. Mech. Rev. 54, 483–502.
Ryvkin, M., Aboudi, J., 2011. Crack resistance in two-dimensional periodic materials of medium and low porosity. Eng. Fract. Mech. 78, 2153–2160.
Selvadurai, A.P.S., Mahyari, A.T., 1998. Computational modelling of steady crack extension in poroelastic media. Int. J. Solids Struct. 35, 4869–4885.
Shafiro, B., Kachanov, M., 1997. Materials with fluid-filled pores of various shapes: effective elastic properties and fluid pressure polarization. Int. J. Solids Struct. 34, 3517–3540.
Shao, Q., Fernández-González, R., Mikdam, A., Bouhala, L., Younes, A., Núñez, P., Belouettar, S., Makradi, A., 2014. Influence of heat transfer and fluid flow on crack growth in multilayred porous/dense materials using XFEM: application to solid oxide fuel cell like material design. Int. J. Solids Struct. 51, 3557–3569.
Shojaei, A., Dahi Taleghani, A., Li, G., 2014. A continuum damage failure model for hydraulic fracturing of porous rocks. Int. J. Plast. 59, 199–212.
Smith, E., 2005. Underpinning of a simple blunt flaw fracture initiation relation. Int. J. Fract. 131, 401–405.
Tada, H., Paris, P.C., Irwin, G.R., 2000. The stress analysis of cracks handbook. ASME press, New York.
Tokiwa, T., Tsusaka, K., Matsubara, M., Ishikawa, T., Ogawa, D., 2013. Formation mechanism of extension fractures induced by excavation of a gallery in soft sedimentary rock, Horonobe area, Northern Japan. Geosci. Front. 4, 105–111.
Tsusaka, K., Tokiwa, T., 2013. Influence of fracture orientation on excavatability of soft sedimentary rock using a hydraulic impact hammer: a case study in the Horonobe Underground Research Laboratory. Tunn. Undergr. Sp. Tech. 38, 542–549.
Vermorel, R., Pijaudier-Cabot, G., 2014. Enhanced continuum poromechanics to account for adsorption induced swelling of saturated isotropic microporous materials. Eur. J. Mech. A/Solids 44, 148–156.
Wang, H.F., 2000. Theory of Linear Poroelasticity: With Applications to Geomechanics and Hydrogeologoy. Princeton University Press.
Zybell, L., Hütter, G., Linse, T., Mühlich, U., Kuna, M., 2014. Size effects in ductile failure of porous materials containing two populations of voids. Eur. J. Mech. A/Solids 45, 8–19.

Please cite this article in press as: Liu, M., Chen, C. A micromechanical analysis of the fracture properties of saturated porous media. Int. J. Solids Struct. (2015), http://dx.doi.org/10.1016/j.ijsolstr.2015.02.031